

## MIT Open Access Articles

*Geometric Effect of Asperities on Shear Mechanism of Rock Joints*

The MIT Faculty has made this article openly available. **Please share** how this access benefits you. Your story matters.

**Citation:** Fathi, Ali, Zabihallah Moradian, Patrice Rivard, Gérard Ballivy, and Andrew J. Boyd. "Geometric Effect of Asperities on Shear Mechanism of Rock Joints." *Rock Mechanics and Rock Engineering* 49, no. 3 (August 1, 2015): 801–820.

**As Published:** <http://dx.doi.org/10.1007/s00603-015-0799-6>

**Publisher:** Springer Vienna

**Persistent URL:** <http://hdl.handle.net/1721.1/104448>

**Version:** Author's final manuscript: final author's manuscript post peer review, without publisher's formatting or copy editing

**Terms of Use:** Article is made available in accordance with the publisher's policy and may be subject to US copyright law. Please refer to the publisher's site for terms of use.



# Geometric Effect of Asperities on Shear Mechanism of Rock Joints

Ali Fathi<sup>1</sup> · Zabihallah Moradian<sup>1,2</sup> · Patrice Rivard<sup>1</sup> · Gérard Ballivy<sup>1</sup> · Andrew J. Boyd<sup>3</sup>

Received: 7 October 2014 / Accepted: 21 July 2015 / Published online: 1 August 2015  
© Springer-Verlag Wien 2015

**Abstract** Three-dimensional tracking of changes of asperities is one of the most important ways to illustrate shear mechanism of rock joints during testing. In this paper, the changes of the role of asperities during different stages of shearing are described by using a new methodology for the characterization of the asperities. The basis of the proposed method is the examination of the three-dimensional roughness of joint surfaces scanned before and after shear testing. By defining a concept named ‘tiny window’, the geometric model of the joint surfaces is reconstructed. Tiny windows are expressed as a function of the  $x$  and  $y$  coordinates, the height ( $z$  coordinate), and the angle of a small area of the surface. Constant normal load (CNL) direct shear tests were conducted on replica joints and, by using the proposed method, the distribution and size of contact and damaged areas were identified. Image analysis of the surfaces was used to verify the results of the proposed method. The results indicated that the proposed method is suitable for determining the size and distribution of the contact and damaged areas at any shearing stage. The geometric properties of the tiny windows in the pre-peak, peak, post-peak softening, and residual shearing stages were investigated based on their angle and height. It was found that tiny windows that face the shear direction, especially the steepest ones, have a primary

role in shearing. However, due to degradation of asperities at higher normal stresses and shear displacements, some of the tiny windows that do not initially face the shear direction also come in contact. It was also observed that tiny windows with different heights participate in the shearing process, not just the highest ones. Total contact area of the joint surfaces was considered as summation of just-in-contact areas and damaged areas. The results of the proposed method indicated that considering differences between just-in-contact areas and damaged areas provide useful insights into understanding the shear mechanism of rock joints.

**Keywords** Rock joints · Asperities · Shear mechanism · Roughness · Contact areas · Damaged areas · Tiny windows

## 1 Introduction

Understanding the shear mechanism of rock joints is a key step for designing geotechnical projects that include discontinuities. The shear mechanism of joints is strongly affected by the joint roughness, the loading conditions, and the mechanical properties of the rock (Barton 1973; Kulatilake et al. 1995; Re and Scavia 1999; Gentier et al. 2000; Yang et al. 2001; Lopez et al. 2003). The shear mechanism of rock joints is the basis of constitutive models for predicting the shear strength of rock joints. Some of the early researchers who considered shear mechanism of asperities in the description of shear strength were Patton (1966), Rengers (1970), Ladany and Archambault (1970), and Barton (1973). Patton (1966) studied the shear behavior of ‘‘saw-tooth’’ joints. Patton observed that sliding occurred along the intact asperity when the effective normal stresses were low and the effect of the intact

✉ Ali Fathi  
ali.fathi@usherbrooke.ca

<sup>1</sup> Département de Génie Civil, Université de Sherbrooke, 2500 Boul. de l’université, Sherbrooke, Québec J1K 2R1, Canada

<sup>2</sup> Department of Civil and Environmental Engineering, Massachusetts Institute of Technology (MIT), 77 Massachusetts Avenue, Cambridge, MA 02139, USA

<sup>3</sup> Department of Civil Engineering, McGill University, 817 Sherbrooke Street West, Montreal, Québec H3A 0C3, Canada

asperities disappeared due to the shearing of the asperity when effective normal stresses were high. He proposed the following bilinear failure criterion:

$$\tau_f = \sigma_n' \cdot \tan(\phi_b + i) \quad (\text{for low effective normal stresses}),$$

$$\tau_f = c_x + \sigma_n' \cdot \tan(\phi_r) \quad (\text{for high effective normal stresses}),$$

where  $\tau_f$  is the peak shear strength,  $\sigma_n'$  the normal stress,  $\phi_b$  the basic friction angle,  $\phi_r$  the residual friction angle,  $c_x$  the cohesion when the asperities are sheared, and  $i$  the angle of the “saw-tooth” asperities with respect to the shear direction. According to Ladanyi and Archambault (1970), Patton’s criterion has some limitations such as similarity between the geometry of the asperities at failure and at the beginning of shearing, difficulty to define the average inclination angle  $i$  of the asperities and the cohesion intercept for natural joints. In an attempt to address the Patton criterion’s shortcomings, Ladanyi and Archambault (1970) proposed a new criterion. They defined  $a_s$  to be the area where shearing through the asperities takes place. Over the rest of the surface ( $1 - a_s$ ), the asperities are assumed to slide over each other without creating damage. They considered the rate of dilation at failure ( $\dot{v}$ ) and the shear area ratio ( $a_s$ ) of the joint surface in their criterion:

$$\tau = \frac{\sigma(1 - a_s)(\dot{v} + \tan \phi_u) + a_s(\sigma \cdot \tan \phi_i + \eta \cdot c_i)}{1 - (1 - a_s) \cdot \dot{v} \cdot \tan \phi_f},$$

where  $\phi_u$  is the frictional resistance along the contact surfaces of the asperities,  $\phi_i$  the friction angle of the intact rock material,  $\eta$  the degree of interlocking,  $c_i$  the cohesion of the intact rock material, and  $\phi_f$  the statistical average value of friction angle that is assessed when sliding occurs along the irregularities of different orientations. The main problem with this criterion is the variation of the parameters that causes a complicated determination of the shear strength. According to Seidel and Haberfield (1995), the original analysis from Ladanyi and Archambault (1970) was restricted to joints with rigid asperities. Asperity sliding can only occur on asperities with a slope angle equal to the critical slope and asperities with lower slope angles cannot be in contact in the shearing. Seidel and Haberfield (1995) showed that both the elastic and plastic behavior of the joint asperity must be taken into account. They indicated that in weak rocks where plastic behavior is more significant, the dilation rate is less than the asperity angle. Therefore, the effective asperity angle is less than the angle proposed by Ladanyi and Archambault (1970).

A practical alternative for predicting the shear strength of the rough joints was proposed by Barton (1973). He was the first to take into account the influence of the natural roughness on the joint strength. Barton (1973) and Barton

and Choubey (1977) studied the behavior of several joints and proposed an empirical shear failure criterion:

$$\tau = \sigma_n \tan\left(\phi_b + \text{JRC} \log_{10}\left(\frac{\text{JCS}}{\sigma_n}\right)\right),$$

where  $\phi_b$  is the basic friction angle, JRC (joint roughness coefficient) a parameter that represents the roughness of the joint and JCS (Joint Compressive Strength) the compressive strength of the rock on the joint surface. Barton and his co-workers did not consider the effect of contact area between the upper and lower joint halves in their shear criterion. Therefore, a modification of Barton’s criterion was suggested by Zhao (1997), who added a joint matching coefficient (JMC) to the Barton criterion:

$$\tau_p = \sigma_n \cdot \tan\left(\phi_b + \text{JMC} \cdot \text{JRC} \cdot \log_{10}\left(\frac{\text{JCS}}{\sigma_n}\right)\right).$$

The parameter JMC ranged from zero to one representing the contact area of the joint surface. The JMC is one when the joint surfaces are perfectly matched and is zero for a maximal unmated joint.

Hutson and Dowding (1990) suggested that asperity degradation is a function of loading conditions, joint roughness, and uniaxial compressive strength of rock. They characterized the asperity behavior as that being under high and low normal stresses. Under high normal stresses, asperity degradation can occur during small shear displacements. Conversely, under low normal stresses, asperity degradation can arise if the shear displacement is large enough. Gentier et al. (2000) developed a method using image processing techniques. They showed that the mechanical behavior of joints is strongly linked to the geometry of asperities. The size, shape, and distribution of damaged areas are related to the shear direction, normal stress, and shear displacement. They found that asperity damage is most likely to occur in areas where the local dip direction is close to the shear direction and on asperities with the steepest slopes. Seidel and Haberfield (2002) developed theoretical models to predict the shear behavior of soft rock joints. Their model is composed of two independent mechanisms: initial sliding along the surface of the asperities and then simultaneous shearing through all of the intact asperities. The consequence of this sliding is joint dilation and stress localization on the steepest asperities in contact. The steepest asperities are sheared when the shear stresses exceeds the asperities’ strength. Then the shear stresses are shed to the next steepest asperities and these asperities control the dilation until they also fail in shearing. Grasselli and Egger (2003) introduced quantitative three-dimensional surface parameters into a shear strength criterion. They stated that degradation is more likely to occur in steeper asperities. Therefore, instead of considering the whole

contact area between surfaces, an effective contact area should be considered in the shearing process. They explained that effective contact areas only occur in asperities that face the shear direction. Moreover, they stated that only the steepest asperities are in contact in the shearing process and are deformed, sheared or crushed depending on the applied normal load. Barbosa (2009) described the behavior of joints in the field based on the behavior of small-scale samples and the geometry of large-scale waviness. He categorized the shear mechanism of the pre-peak shear strength into elastic and plastic stages. In the elastic stage there is neither degradation nor dilation, thus, there is no decrement in the asperities angles. After the elastic stage, the joint starts to slide over the asperities (pre-peak plastic stage). At this stage, degradation and dilation are initiated. Based on asperity angles, Park and Song (2013) characterized the joint surfaces by introducing a concept named ‘micro-slope angle’ which is an extension of the ‘apparent dip angle’ suggested by Grasselli and Egger (2003). By back-analyzing the shear and normal displacements obtained from laboratory shear tests and the micro-slope angle concept, Park and Song (2013) introduced a numerical method to determine the contact areas of a rock joint under normal and shear load. They showed that most of the contact areas occur in the regions facing the shear direction, and the asperities with flatter slopes were less likely to come into contact.

Summarizing this previous research, one can state that initial sliding and then simultaneous shearing of asperities are most likely to occur on the steepest asperities that are facing the shear direction. Moreover, size, shape, and distribution of contact areas are related to the geometry of asperities, loading conditions, mechanical parameters of the rock, and shear displacement (Ladanyi and Archambault 1970; Hutson and Dowding 1990; Seidel and Haberfield 1995, 2002; Gentier et al. 2000; Grasselli and Egger 2003; Misra 2002; Karami and Stead 2008; Park and Song 2013). In this paper, a new mathematical method is presented in the form of a software to characterize the joint surfaces. The in-contact asperities in the pre-peak, the post-peak strain-softening, and the residual stages of the shearing process were identified and characterized by considering not only their angle, but also their height, and considering both height and angle simultaneously, to find out which types of asperities among the steepest ones have the greatest effect on the shear mechanism.

## 2 Specimen Preparation and Experimental Procedure

One advantage of using joint replicas is that they make it possible to study the effect of one specific factor on the shear mechanism of the joints while the other factors do not

change. Thus, the rectangular-shaped joint replicas were prepared by pouring non-shrinking cement mortar on a fresh joint surface of an artificially split granite block to reproduce its roughness.

A rectangular wooden mold, with an internal dimension of 140 × 140 mm, was fixed on the granite joint surface and, after spraying a form release agent (to allow easy detachment of the replica), grout was poured into the mold (Fig. 1a). An appropriate mortar recipe (Water and SikaGrout 212 at a ratio of 0.18) was selected to fabricate the mortar specimens. The grain sizes of the mortar were small enough to sufficiently reproduce the details of the granite surface roughness (Fig. 1b). Then, a taller mold was made and the first half of the specimen was fixed within it, while the second half of the specimen was formed by pouring mortar onto the surface of the first half. A total of 38 specimens were prepared using this method. According to the roughness parameters calculated for granite joint and specimen surfaces, the roughness of specimens was acceptably close to the roughness of original granite surface (Table 1). Some cylindrical specimens were also made from the mortar used for fabricating the joint specimens. After 65 days, the uniaxial compressive strength and tensile strength of these specimens were measured as 83 and 4.4 MPa, respectively.

A profilometer laser scanner (Kreon Zephyr© 25) was used to acquire 3D coordinates of the joint surfaces. Rousseau et al. (2012) discuss the advantages and limitations of this scanner. The maximum resolution of the laser profilometer was 72 μm for the *x* and *y* axes, and 16 μm for the *z* axis. Scans were performed before and after each shear test. The laser profilometer scans joint surfaces at a high data density and makes them available as a cloud of points (about 25,000,000 points for each specimen in this study). The number of this dense cloud of points needs to be reduced by gridding to calculate the roughness parameters and reconstruct the joint surface. The sampling interval effect depicted in Fig. 2 has to be considered in gridding the cloud of points. As it can be seen in Fig. 2, at larger sampling intervals (4a), some high-frequency components may be lost and the reconstructed surface may be smoother. As a result, the sampling interval is a factor that has to be carefully taken into account for reconstructing the joint surface by numerical methods.

In the current study, roughness parameters such as  $Z_2$ ,  $R_p$ , and  $R_s$  (Fig. 3) were calculated at different intervals to reduce the sampling interval effect.  $Z_2$  represents the root mean square of the first height derivative in the 2D profile. For a 2D profile,  $Z_2$  is defined as (Myers 1962):

$$Z_2 = \left[ \frac{1}{M(Dx)^2} \sum_{i=1}^M (z_{i+1} - z_i)^2 \right]^{0.5} \quad \text{and} \quad Dx = x_{i+1} - x_i,$$

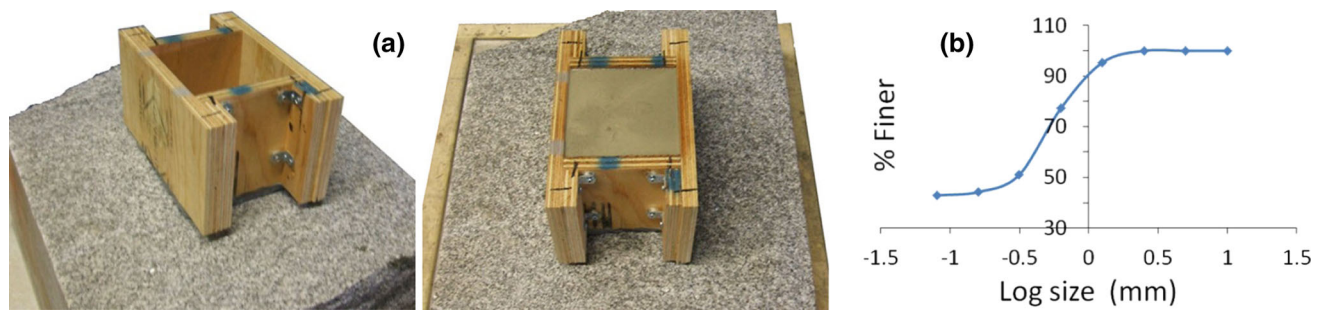


**Fig. 1** a Manufacturing of the mortar replicas, b diagram of the SIKA grading test

**Table 1** Summary of roughness parameters obtained from upper half of specimens

Dimension	Parameter	Interval (mm)	Original granite surface	Specimens										
				A126	A127	A129	A135	A137	A139	A141	A142	A144	A145	
2D	$Z_2$	1	0.188	0.185	0.180	0.181	0.181	0.182	0.181	0.181	0.181	0.180	0.179	0.182
		0.8	0.199	0.194	0.190	0.199	0.199	0.195	0.194	0.193	0.192	0.194	0.196	
		0.6	0.210	0.205	0.200	0.201	0.200	0.202	0.201	0.201	0.203	0.201	0.200	
		0.5	0.217	0.211	0.207	0.206	0.205	0.206	0.207	0.206	0.207	0.206	0.209	
		0.4	0.226	0.218	0.214	0.214	0.213	0.215	0.214	0.214	0.213	0.211	0.216	
		0.2	0.254	0.244	0.247	0.249	0.249	0.245	0.244	0.245	0.246	0.245	0.243	
		0.1	0.386	0.333	0.374	0.394	0.387	0.381	0.368	0.382	0.375	0.371	0.363	
	$R_p$	1	1.020	1.009	1.016	1.016	1.016	1.014	1.015	1.015	1.015	1.017	1.014	1.015
		0.8	1.022	1.018	1.017	1.017	1.017	1.016	1.018	1.017	1.016	1.017	1.017	
		0.6	1.026	1.020	1.019	1.019	1.019	1.021	1.020	1.020	1.019	1.018	1.019	
		0.5	1.025	1.021	1.020	1.020	1.020	1.021	1.021	1.021	1.021	1.020	1.021	
		0.4	1.029	1.023	1.022	1.022	1.022	1.022	1.022	1.022	1.021	1.022	1.023	
		0.2	1.033	1.029	1.029	1.028	1.028	1.028	1.028	1.028	1.027	1.028	1.028	
		0.1	1.073	1.058	1.061	1.063	1.061	1.062	1.062	1.061	1.059	1.062	1.062	
3D	$R_s$	1	1.017	1.016	1.016	1.016	1.015	1.016	1.016	1.016	1.015	1.016	1.016	
		0.8	1.019	1.017	1.017	1.017	1.017	1.017	1.018	1.017	1.017	1.017		
		0.6	1.020	1.020	1.019	1.019	1.019	1.020	1.019	1.020	1.019	1.019		
		0.5	1.022	1.021	1.021	1.020	1.020	1.021	1.020	1.020	1.020	1.020		
		0.4	1.022	1.022	1.022	1.021	1.021	1.022	1.020	1.021	1.020	1.021		
		0.2	1.024	1.024	1.023	1.023	1.023	1.024	1.023	1.023	1.022	1.023		
		0.1	1.071	1.059	1.061	1.063	1.060	1.061	1.061	1.061	1.060	1.062	1.061	

where  $Dx$  is the equal interval between sampling points,  $M$  is the number of intervals, and  $(x_i, z_i)$  and  $(x_{i+1}, z_{i+1})$  are coordinates of the  $(i)$ th and  $(i + 1)$ th sampling points, respectively.

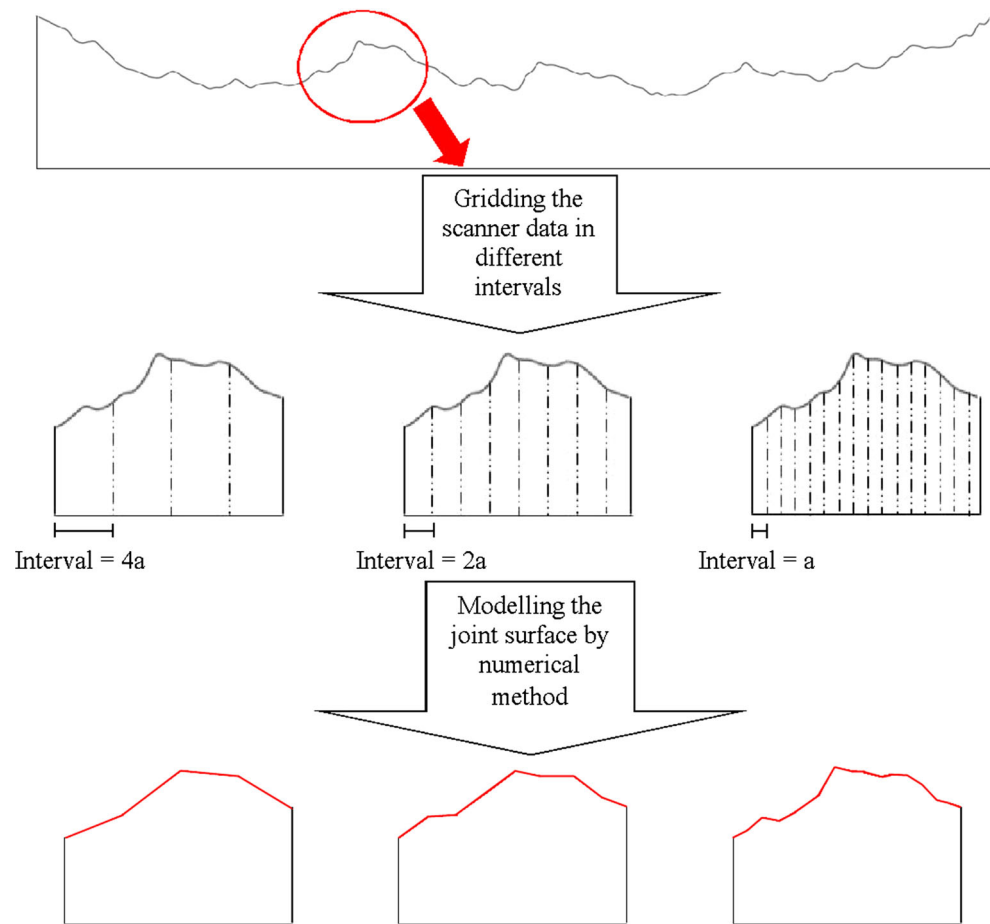
$R_p$  is defined as the ratio of the true profile length to its projected length in the joint plane  $L$ .  $R_s$  is the 3D analog of  $R_p$ , defined as the ratio of true surface area,  $A_t$ , to its projected surface area,  $A_n$  (El Soudani 1978):

$$R_p = \frac{\sum_{i=1}^{n-1} [(x_{i+1} - x_i)^2 + (z_{i+1} - z_i)^2]^{0.5}}{L},$$

$$R_s = \frac{A_t}{A_n}.$$

The roughness parameters that were calculated considering various sampling intervals are presented in Table 1. The values of 2D roughness parameters in Table 1 are averages of the roughness parameters calculated for 140 isometric profiles. The profiles were parallel to the shear direction with 1 mm interval. For each profile, the 2D roughness parameters were calculated with sampling intervals from 0.1 to 1 mm. For 3D roughness parameter ( $R_s$ ), the true surface area of joint specimens was calculated

**Fig. 2** The effect of three sampling intervals on the roughness parameters and profile reconstruction



according to the number and angles of tiny windows with dimensions from  $0.1 \text{ mm} \times 0.1 \text{ mm}$  to  $1 \text{ mm} \times 1 \text{ mm}$ .

The 2D roughness parameters were also calculated at different directions with sampling interval of  $0.5 \text{ mm}$ . Figure 4 presents the values of  $Z_2$  and  $R_p$  calculated for different directions. The zero direction is parallel to the shear direction.

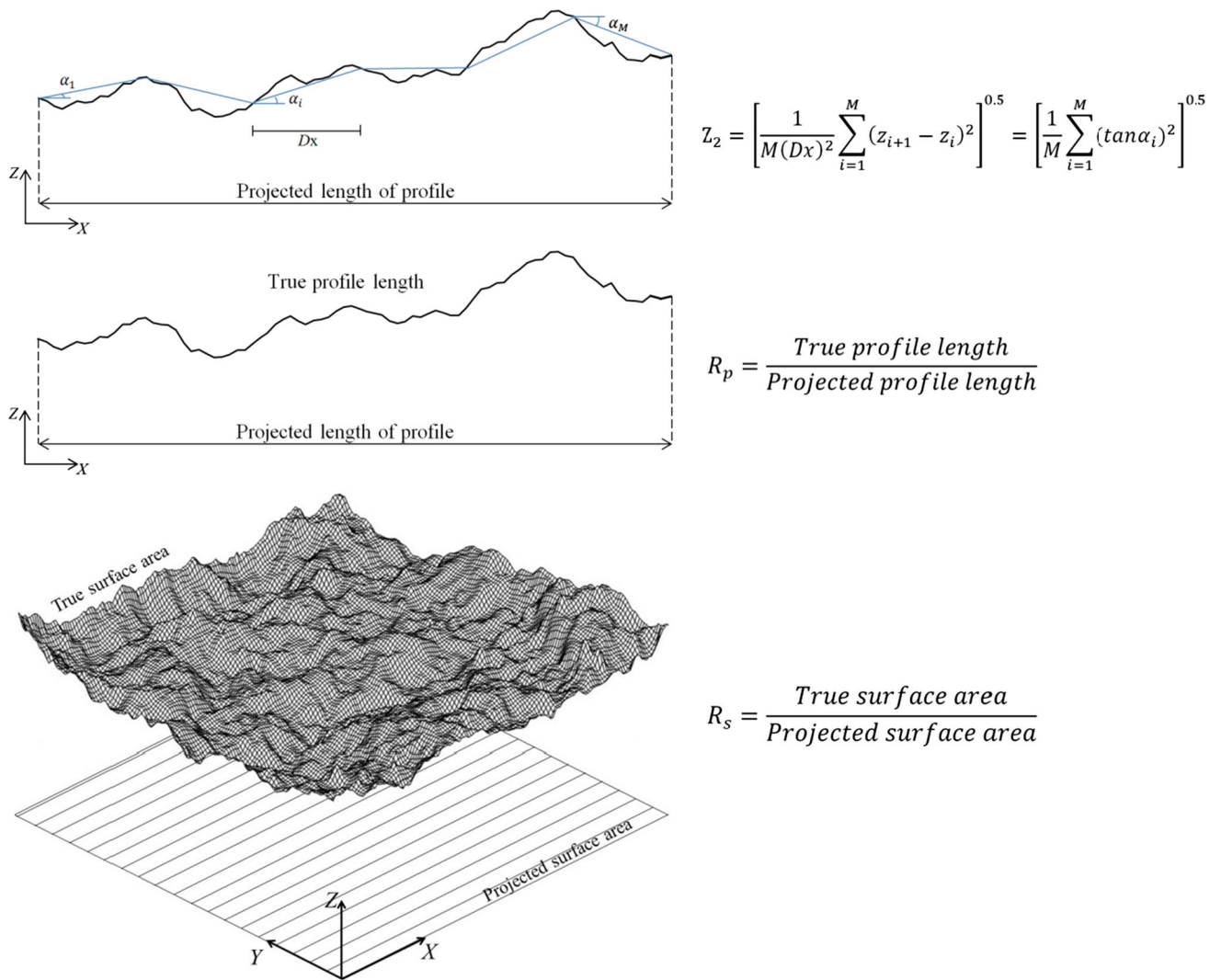
The shear tests were conducted using a material testing system (MTS) press, at the Laboratory of Rock Mechanics, Université de Sherbrooke. This apparatus was developed by Mouchaorab and Benmokrane (1994). The MTS press is servo-controlled and has a capacity of  $2670 \text{ kN}$  (Fig. 5). The normal and shear loads were measured directly by the respective load cells. Normal and shear displacements were measured using four LVDTs and one extensometer (run of  $25 \pm 0.05 \text{ mm}$ ) with high-precision repeatability.

### 3 Description of the New Method for Joint Surface Characterization

In the method proposed here, the joint surface was divided into a large number of tiny windows (Fig. 6). Each tiny window was expressed as a function of  $x$  and

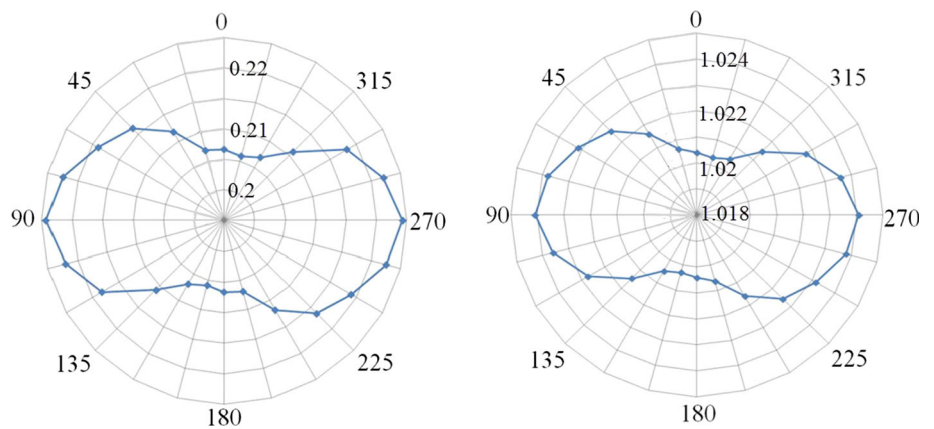
$y$  coordinates, as well as the height and angle of a small area of the joint surface. Several tiny windows may characterize one joint asperity; therefore, a careful consideration must be taken into account with the two concepts of asperity and tiny window. The height of the central point of the tiny window was considered to be the height of the whole tiny window. The height of tiny windows was calculated from a horizontal plane that passes through the central point of the lowest tiny window. In other words, the height of the lowest tiny window was considered as zero and the heights of the others were measured based on that. The slope of the intersection line of the tiny window plane and a vertical plane passing through the central point of the tiny window and containing the shear direction vector was considered to be the angle of the tiny window (Fig. 6).

Custom software was developed based on the proposed method (tiny windows). With this software, detecting contact areas and damaged areas, and characterizing in-contact tiny windows was possible during different stages of shearing. These objectives were achieved based on the following steps:



**Fig. 3** Roughness parameters defined in 2D ( $Z_2$  and  $R_p$ ) and 3D ( $R_s$ )

**Fig. 4** Values of  $Z_2$  (left) and  $R_p$  (right) calculated for different directions (Specimen A127) with 0.5 mm intervals. The zero direction is parallel to the shear direction



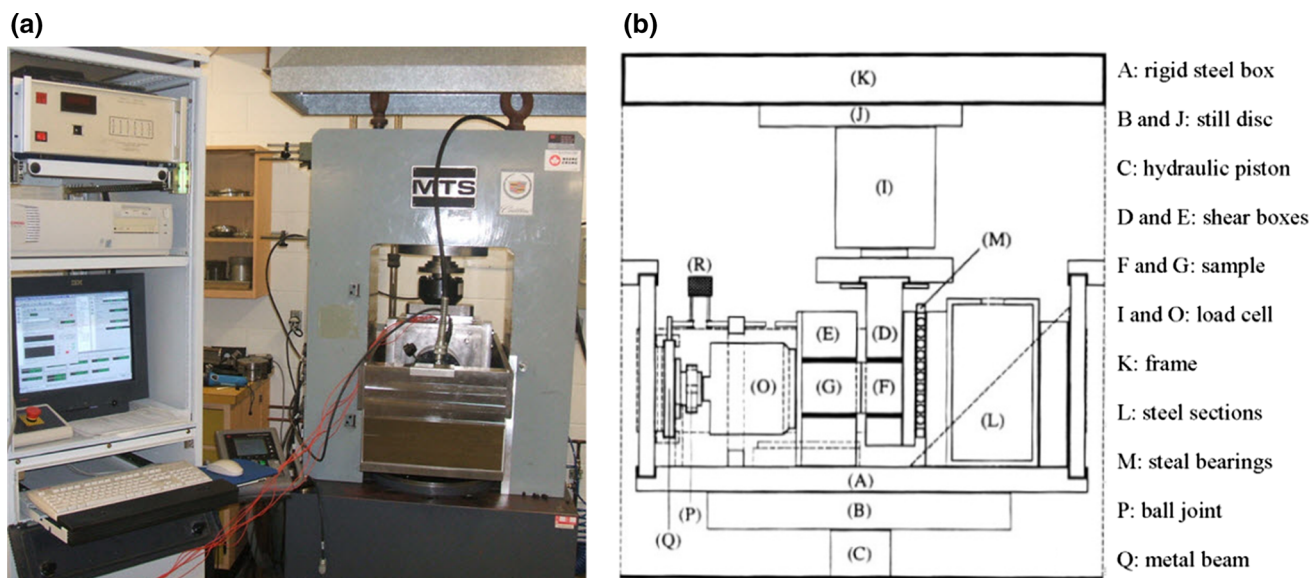


Fig. 5 a MTS press system, b diagram of vertical section of the shear apparatus

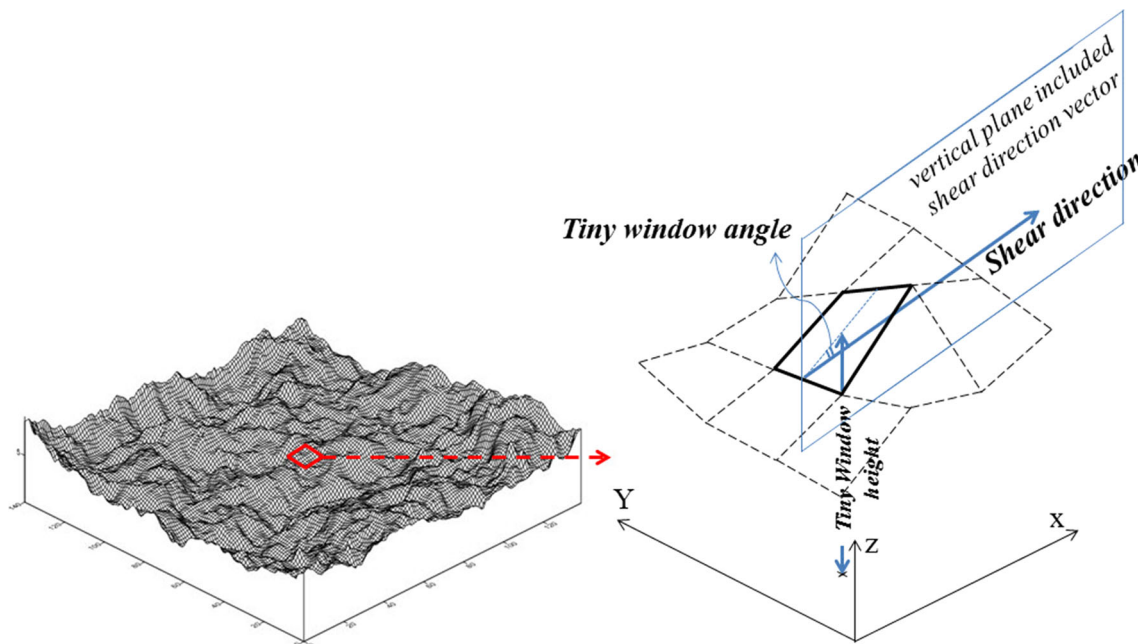


Fig. 6 Joint surface divided into a large number of tiny windows. The tiny windows size will vary depending on the accuracy required

- Before test
- The upper and lower surfaces of the replica joint were scanned with high precision. In the current study, joints were scanned and gridded at 0.1, 0.2, 0.4, 0.5, 0.6, 0.8 and 1 mm intervals.
- Given that more details are detected with smaller intervals (Fig. 2), when the sampling interval decreased from 1 to 0.2 mm, the roughness parameters slightly increased (Table 1). This roughness increment was followed by an irregular increase from 0.2 into 0.1 mm

- interval. Therefore, to avoid this irregularity, a sampling interval of 0.2 mm was considered as the minimum sampling interval for reconstructing the joint surfaces.
- Considering the sampling interval of 0.2 mm, the joint surface was divided into 490,000 tiny windows (0.2 × 0.2 mm). The angle and height of each tiny window were calculated and linked to the related x and y coordinates.
- To detect contact and damaged areas, the coordinates of both surfaces were defined in the same system



(Fig. 7). For this purpose, a series of reference targets were attached around the shear box and scanned with the joint surface. These reference targets were considered as benchmarks for defining the coordinates of the surfaces in the same system (Fig. 8). Considering the sample preparation method, it was assumed that the upper and lower replica surfaces are completely matched at the initial stage of shearing.

- After test
- After each shear displacement increment, the new coordinates of the upper surface were recalculated using measured shear and normal displacements (Fig. 7).

$$X_{iup} = x_{iup} + dx,$$

$$Y_{iup} = y_{iup},$$

$$Z_{iup} = z_{iup} + dz,$$

where  $dx$  is the shear displacement,  $dz$  is the normal displacement and,  $x_{iup}, y_{iup}, z_{iup}$ , and  $X_{iup}, Y_{iup}, Z_{iup}$  are the initial and the new coordinates of the  $i^{\text{th}}$  point on the upper surface, respectively.

- The new upper surface was meshed with the same interval as the lower surface. The grid coordinates of the lower and upper meshes should be face to face (Fig. 7).
- The lower and upper face to face tiny windows (one from the lower surface and another from the upper) were compared considering their height ( $z$  coordinate) to determine whether the two tiny windows were still in contact after each shear displacement (Fig. 9).
- If  $Z_{w_i,up} - Z_{w_i,lw} < 0$ , tiny windows are in contact and asperities have been damaged.
- If  $Z_{w_i,up} - Z_{w_i,lw} = 0$ , tiny windows are just in contact, and no damage occurs.

- If  $Z_{w_i,up} - Z_{w_i,lw} > 0$ , tiny windows are not in contact, where  $Z_{w_i,up}$  and  $Z_{w_i,lw}$  are the height of the  $i^{\text{th}}$  tiny window of the upper and lower surfaces.

These three conditions are shown in a 2D view in Fig. 9. Considering the height difference ( $z$  coordinate) of the face to face tiny windows, the contact area was modeled. Using this method, all tiny windows were identified at different shear displacements, based on their condition: just in contact, in-contact damaged, or not in contact. This allowed us to plot the in-contact tiny windows as well as in-contact damaged areas over the whole scanned surface and then to characterize their properties (angle and height).

The proposed method was employed and the joint surface was characterized with respect to the shear direction (parallel to the direction of  $0^\circ$  in Fig. 4). Figure 10 shows the distribution of the asperity angles for the upper half of Specimen A127. The angle range of tiny windows is from  $-70^\circ$  to  $70^\circ$ . The tiny windows with negative ( $-70^\circ$  to  $0^\circ$ ), small positive ( $0^\circ$ – $15^\circ$ ) and large positive ( $15^\circ$  to  $70^\circ$ ) angles are shown with white, cool and warm colors, respectively. Tiny windows with negative angles (white) cover more joint surface than tiny windows with positive angles (colored). Also, the number of tiny windows with specific height and angle were extracted from the result of the proposed method. Figure 11 displays the frequency plot of height and angle of tiny windows for the upper half of Specimen A127. As can be observed, height and positive angles of the tiny windows varied up to 9.31 mm and  $70^\circ$ , respectively. The majority of tiny windows have angles ranging from  $-20^\circ$  to  $20^\circ$  and heights ranging from 3 to 6 mm. It should be noted that all of these results were obtained before shear testing.

The direct shear test was performed on the replica under 0.8 MPa normal stress. The shear displacement rate was

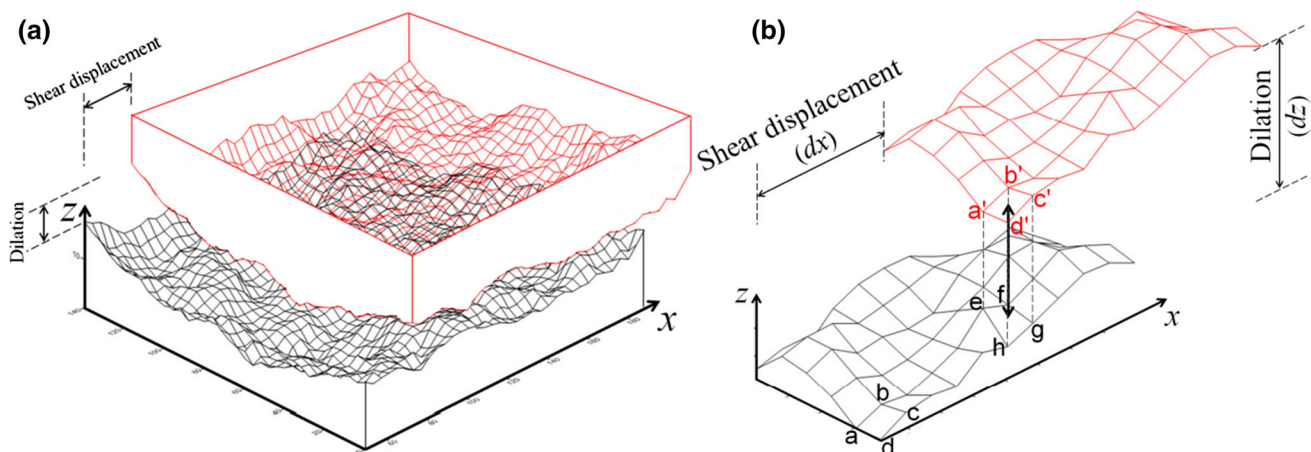


**Fig. 7** **a** The upper surface and lower surface were defined in the same coordinate system. **b** The upper surface was meshed with the same interval as the lower surface

**Fig. 8** Some targets were attached around the *shear box* and were scanned with the joint surface

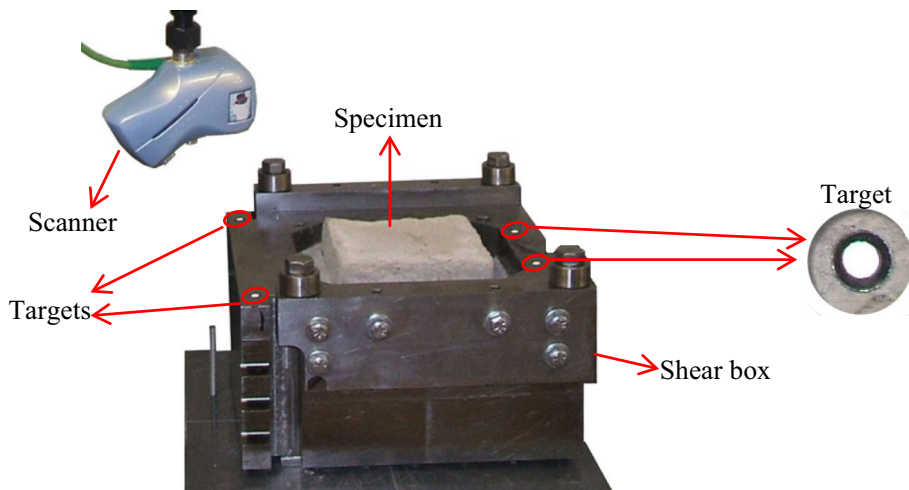
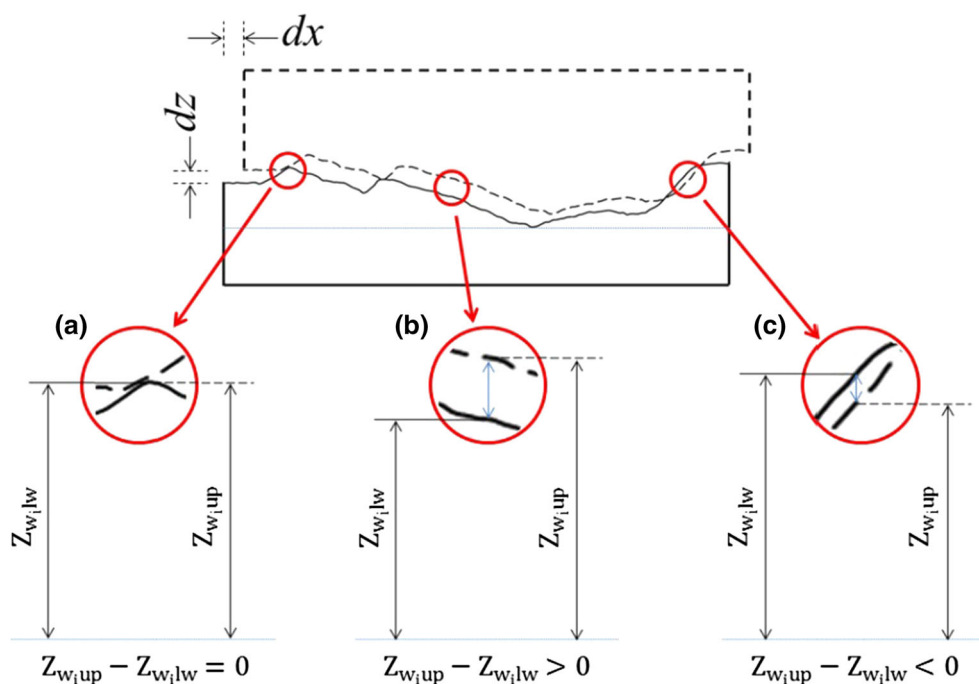


**Fig. 9** Assessment criteria for contact condition: **a** zero = tiny windows are just in contact, **b** positive = tiny windows are not in contact, **c** negative = these windows are in contact and damaged and degradation has occurred. Total contact area is the sum of just-in-contact areas and in-contact damaged areas



0.1 mm/min and the test ended when the shear displacement attained 10 mm. The specimen reached its peak shear strength after a displacement of 0.2 mm. The values of the shear load and the shear and normal displacements were recorded during the test. It was found that a small contraction starts at the initial stage of shearing. The dilation angle increased when shearing starts overriding the asperities. The asperities begin to be sheared with increasing shear displacement and the dilation angle becomes smaller (Fig. 12).

Using the proposed method and measuring the dilation ( $dz$ ) and the shear displacement ( $dx$ ) during shearing, just-in-contact tiny windows and in-contact damaged tiny windows were identified after each 0.2 mm shear

displacement increments. 0.2, 1, and 10 mm shear displacements were chosen as displacements at the peak, during post-peak softening and at the end of residual stages of the shear process, respectively (Fig. 12). Figure 13a1, a2 and a3 show the size and location of the total contact area at 0.2, 1 and 10 mm shear displacements. Total contact area is defined as the summation of just-in-contact areas and in-contact damaged areas. Figure 13b1, b2, and b3 show the cumulative damaged areas up to 0.2, 1, and 10 mm shear displacements. Cumulative damaged areas were chosen to be able to compare them with the images in the next section.

To verify the results of the proposed method for identifying contact areas and damaged areas at different

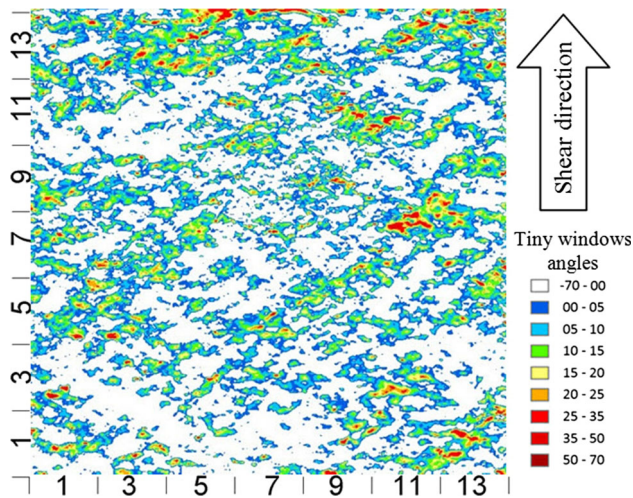


**Fig. 10** Distribution and amount of tiny window angles with respect to the shear direction before shear test (the total number of tiny windows— $0.2 \times 0.2$  mm—is 490,000). The tiny windows with negative ( $-70^\circ$  to  $0^\circ$ ), small positive ( $0^\circ$ – $15^\circ$ ), and large positive ( $15^\circ$ – $70^\circ$ ) angles are shown with white, cool, and warm colors, respectively

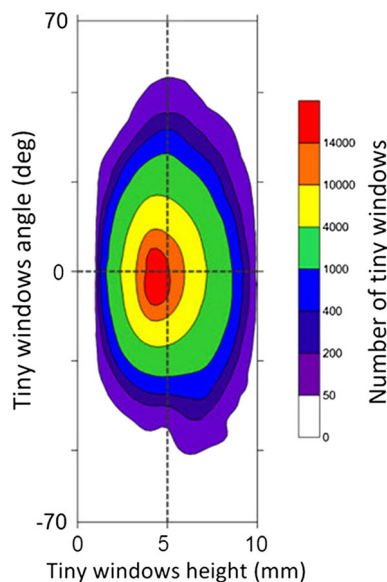


**Fig. 11** Frequency plot of the height and angle of the tiny windows

shearing stages, another method should be employed as a reference. Other researchers have developed several methods that can be used for this purpose:

Methods based on inserting or injecting some materials such as pressure-sensitive film (Nemoto et al. 2009), special metal (Pyrak-Nolte et al. 1987), or epoxy resin (Hakami and Larsson 1996) into the joint interface. The main problem in using pressure-sensitive film methods is the thickness of the material. This problem is exacerbated when the amplitude of the asperities is less than

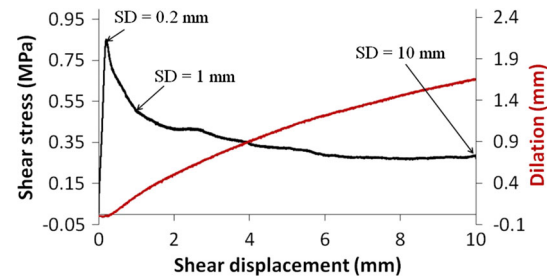


**Fig. 12** Shear stress and dilatation versus shear displacement for Specimen A127 under 0.8 MPa normal stress. 0.2, 1, and 10 mm shear displacements were chosen as displacements at the peak, during post-peak softening and at the end of the residual stages of the shear process

the thickness of the inserted material. Identifying the contact area is only possible after applying normal load using the special metal method or the epoxy resin method. The lack of ability to continuously measure the contact area during the test is another problem in using these methods.

Methods such as the X-ray computer tomography (Re and Scavia 1999) and acoustic emission (AE) (Moradian et al. 2010, 2012) that measure the contact area indirectly. The main drawback of these methods is that they require special equipment and present only qualitative results.

Methods based on numerical calculations (Park and Song 2013). Park and Song (2013) simulated a direct shear test on a rock joint using a bonded particle model in a discrete element code. Their computer code was not available for this work.

Methods based on visual investigation such as image analysis (Gentier et al. 2000; Riss et al. 1997). In these methods, the shear test has to be stopped and the joint surfaces opened for examination and photographing of the joint surfaces. This makes it impossible to continuously measure the contact area during the test. Nevertheless, these methods are the best to directly identify the damaged areas. However, the measurement of the contact area (particularly at the beginning of the test) is somewhat erroneous; in fact, if degradation does not happen, nothing is visible on the images of the joint surfaces and therefore the contact area is not measurable.

To verify the performance of the proposed method, shear tests were conducted under 0.8 MPa normal stress and up to a pre-determined shear displacements and then the tests were stopped while photographs of the joint surfaces were taken for image analysis. The joint surfaces of these replicas were painted to have a clear picture of the damaged areas. Only a thin layer of paint was applied on the replicas' surfaces to avoid undesired effects on the shear tests results.

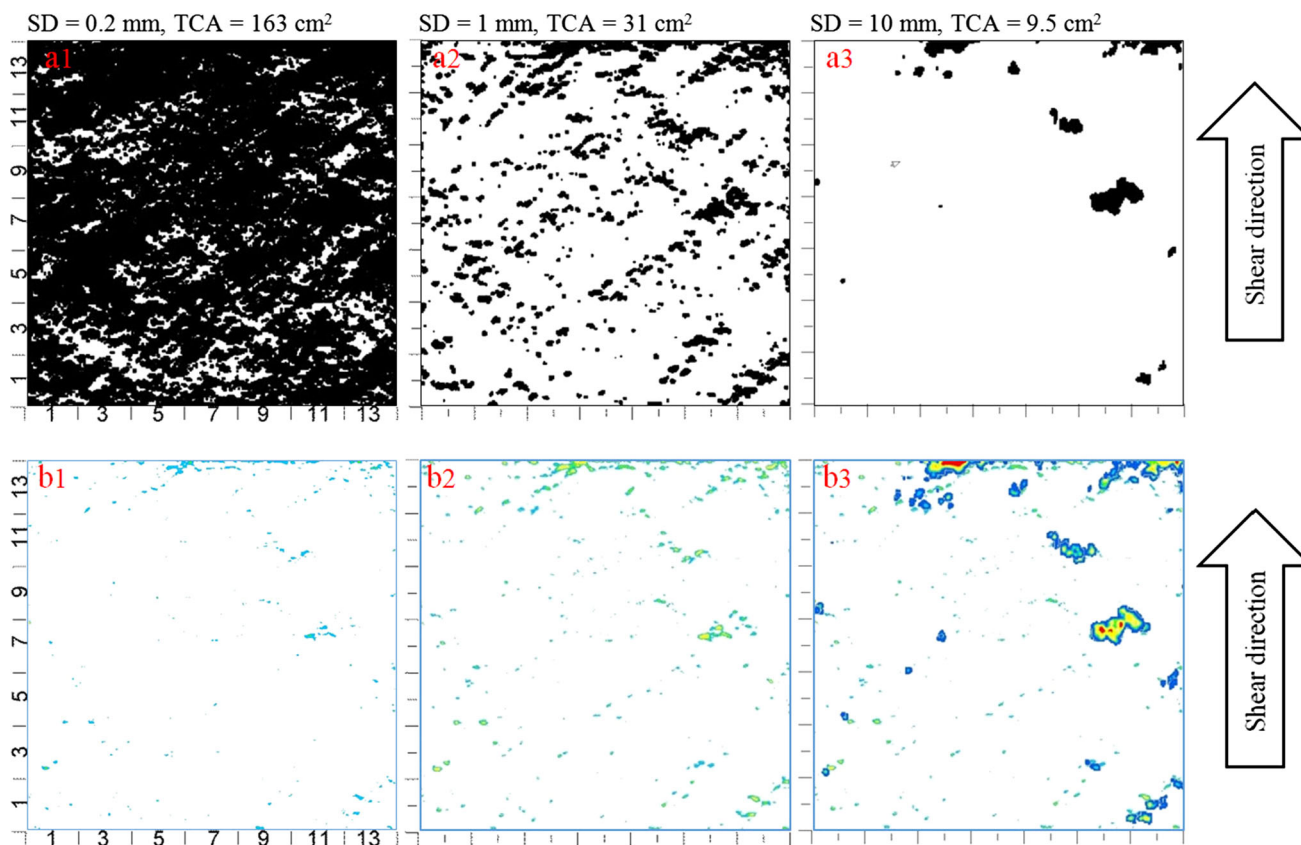


**Fig. 13** Anticipated results using the proposed method. **a** Total contact areas (TCA), *black spots*, and **b** cumulative damaged areas (*colored spots*) occurring during shear tests after *I* 0.2, 2 1, and 3 10 mm shear displacements (SD)

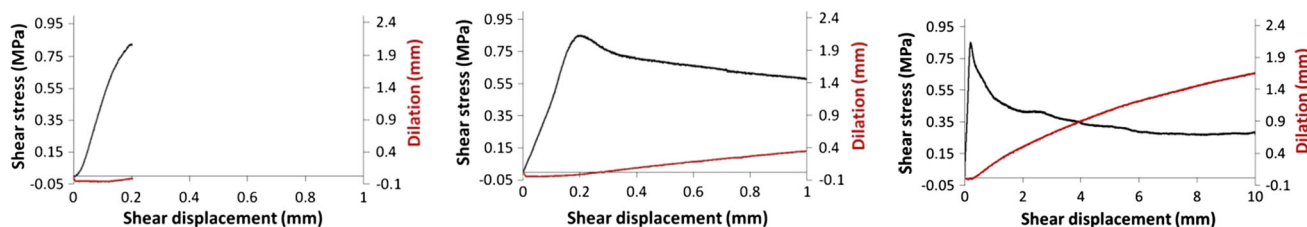


**Fig. 14** Shear stress and dilation vs shear displacement at 0.2, 1, and 10 mm shear displacements

The results of the proposed method for predicting the distribution and size of the damaged areas at three pre-determined shear displacements were compared with image analysis results. The pre-determined shear displacements were chosen at the peak (0.2 mm), during post-peak softening (1 mm) and at the end of the residual stage (10 mm) of the shear stress vs shear displacement graphs (Fig. 14). Photos of the joint surfaces were taken before and after the tests. A wooden frame was employed as the base for the camera and the specimens were always placed in the same position for photography. Therefore, all photos

were taken under identical conditions, which allowed one to directly compare photos. Photos were digitized using 2550 horizontal pixels, 2550 vertical pixels, and 256 gray levels. Figure 15 shows the image analysis results based on the digitized photos that were taken before and after each test. The black spots are representative of the damaged areas.

It can be stated that the locations of estimated damaged areas using the proposed method (Fig. 13b) matched well with those identified by image analysis (black spots) in Fig. 15. These results indicate that the proposed

method is suitable for determining the size and distribution of the damaged areas at any shearing stage. Verifying the predicted just-in-contact areas (Fig. 13a) by the image analysis method was not possible, because just-in-contact areas do not show any significant color change in the photos. Nevertheless, detecting these areas by the proposed method is possible, though the authors believe that further and more detailed studies are necessary.

### 4 Geometric Characterization of Tiny Windows

This part of the study focused on the characterization of the in-contact tiny windows in the shearing process (just-in-contact and in-contact damaged tiny windows—modes a and c in Fig. 9) under different levels of normal stress. Shear tests were conducted under 0.1, 0.2, 0.3, 0.4, 0.5, 0.6, and 0.7 MPa normal stress (Fig. 16). Joints were scanned before and after the shear tests and gridded at 0.2 mm intervals. The joint surfaces were characterized by considering the height and angle of the tiny windows, as well as the shear direction.

### 4.1 Characterization of Tiny Windows Based on Their Angle

Using the proposed method, in-contact tiny windows were identified under different normal stresses and at different shear displacements. In-contact tiny windows were classified into 36 classes of angles from  $-90^\circ$  to  $90^\circ$  with  $5^\circ$  class intervals. The true contact area of each in-contact tiny window is also calculated by considering the dimension ( $I$ ) and angle ( $\alpha_{twi}$ ) of that tiny window (Fig. 17). Therefore, the total contact area for each class of angles ( $A_{\beta to \beta+5}$ ) is calculated by considering the angles ( $\alpha_{twi}$ ) and the number ( $N_{tw}$ ) of tiny windows of that class:

$$\beta < \alpha_{twi} < \beta + 5 \quad A_{\beta to \beta+5} = \sum_{i=1}^{N_{tw}} \frac{I^2}{\cos \alpha_{twi}}$$

$$\beta = -90, -85, -80, -75, \dots, 80, 85.$$

The histograms of the in-contact tiny windows' angles were observed at the initial stage of shearing and after 0.2, 0.4, 1, 6, and 10 mm shear displacements. The histograms for Specimen A135, which was tested under 0.1 MPa normal stress, are shown in Fig. 18. Figure 18a–f shows

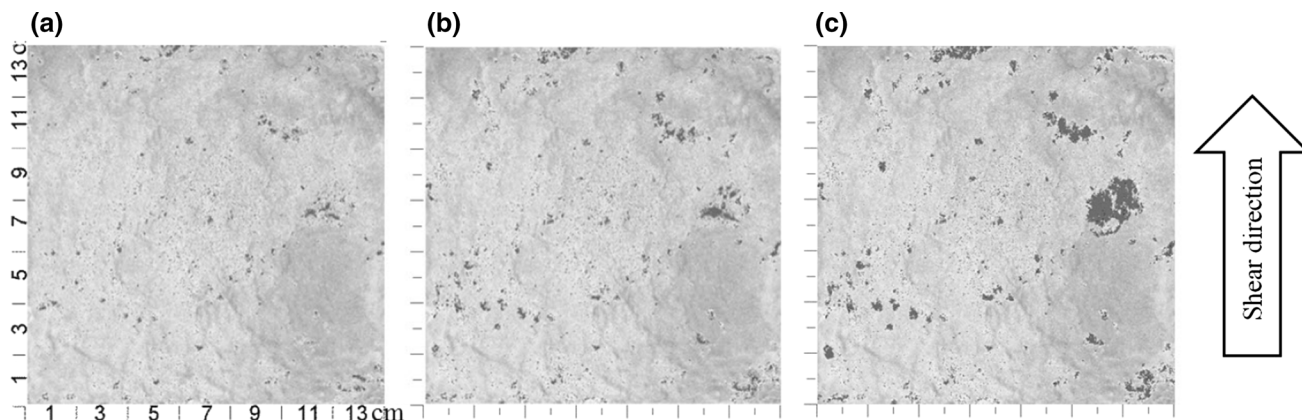


**Fig. 15** Distribution of the damaged areas (black spots) occurring during the shear test after a 0.2, b 1, and c 10 mm shear displacements with image analysis

**Fig. 16** Shear stress and dilation versus shear displacement for shear tests under different levels of normal stress

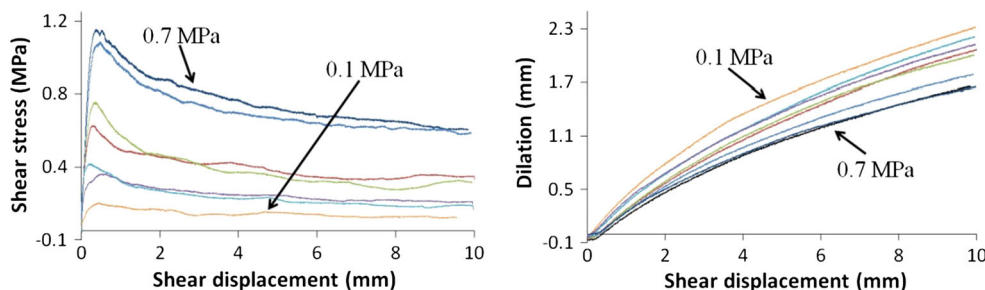


**Fig. 17** The contact area was calculated by considering the angle of each tiny window and the number of tiny windows for each increment

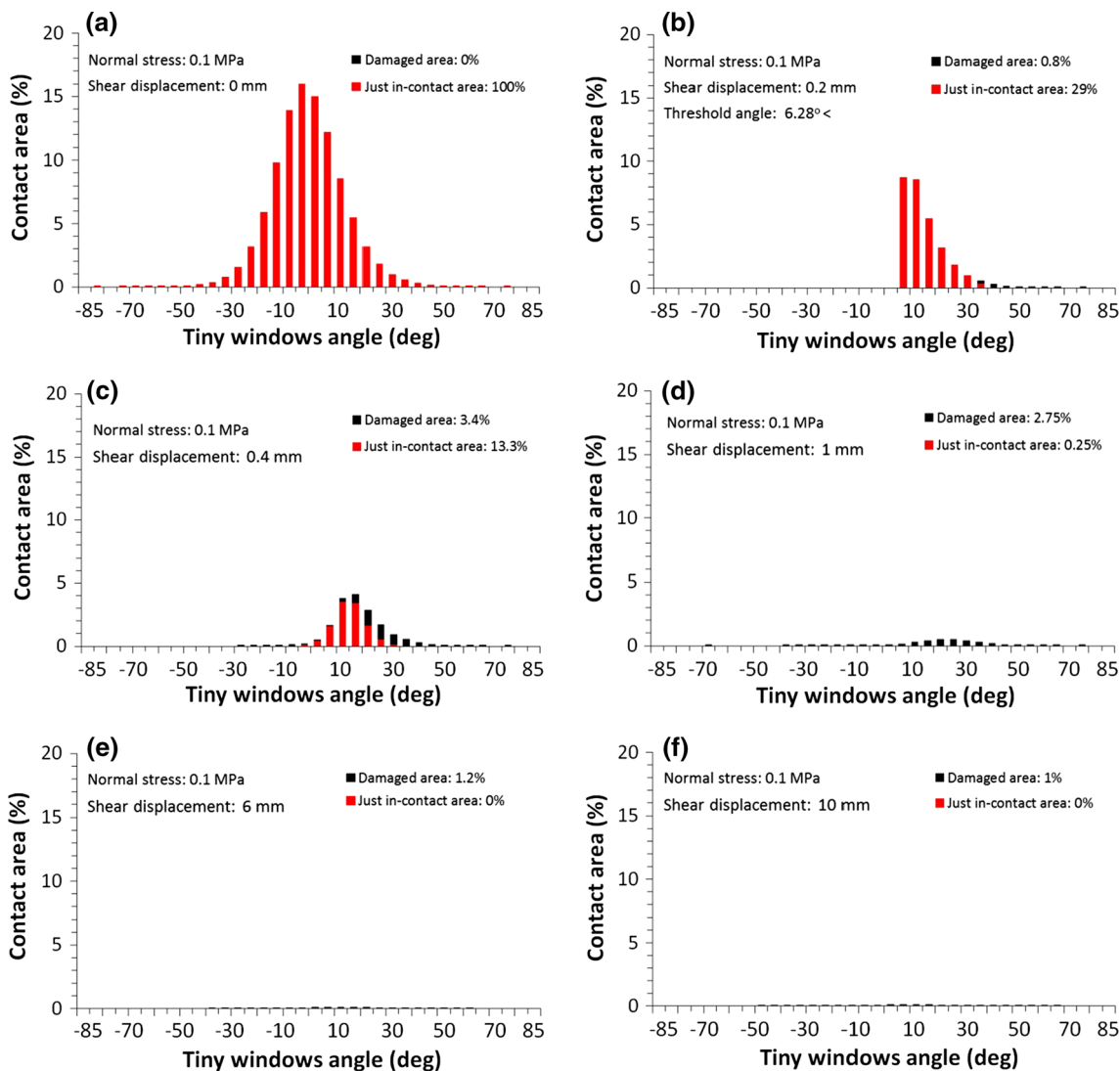
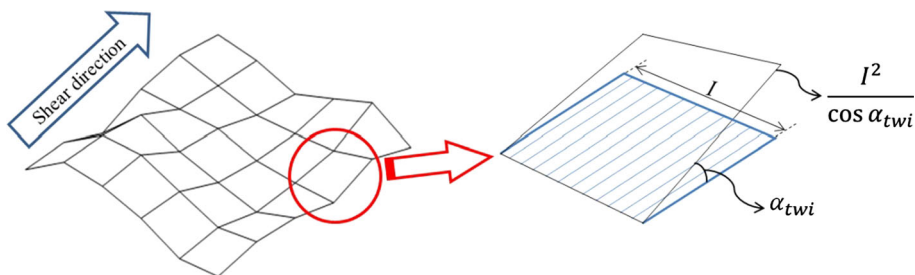


**Fig. 18** Frequency of in-contact tiny windows area versus their angle, under 0.1 MPa normal stress after a 0, b 0.2, c 0.4, d 1, e 6, and f 10 mm shear displacements

the contact area histograms of the tiny windows’ angles after 0, 0.2, 0.4, 1, 6, and 10 mm shear displacement. At the initial stage of shearing, two surfaces of the specimen are just in contact (Fig. 18a). After 0.2 mm shear displacement, the contact area decreased to 29.8 % and degradation started on few tiny windows (Fig. 18b). The

tiny windows that remained in contact were tiny windows with angles greater than  $6.3^\circ$ . The angle of  $6.3^\circ$  as the limit between not-in-contact tiny windows with in-contact tiny windows is defined as an “in-contact threshold angle”. Tiny windows with steeper angles than the in-contact threshold angle are always in contact and degradation may

occur on some of them depending on the normal stress and mechanical properties of the rock material. In this study, another threshold angle (damaged threshold angle) was defined as the limit between in-contact tiny windows and damaged tiny windows. For the test under 0.1 MPa normal stress, this threshold angle was  $38.5^\circ$ .

Figure 19a–f shows the contact area histograms of the tiny windows' angles after 0, 0.2, 0.4, 1, 6, and 10 mm shear displacements when normal stress was 0.7 MPa. Figure 19b shows tiny windows with angles greater than  $2.9^\circ$  (in-contact threshold angle) remain in contact at 0.2 mm shear displacement. Also, degradation started on those tiny windows that had angles greater than  $25^\circ$  (damaged threshold angle). Figure 19c–f also indicates that although at the beginning of the shearing process, only tiny

windows that face the shear direction (positive angle) participate in the shearing process, after increasing shear displacement, some of the tiny windows that do not initially face the shear direction (negative angles) participate as well. Due to degradation, the top parts of asperities are sheared and therefore the angle of their faces may change from negative to positive (Fig. 20). This causes them to participate in the remaining stages of the shearing process.

The contact area of the tested specimens under 0.1, 0.2, 0.3, 0.4, 0.5, 0.6, and 0.7 MPa normal stresses and after 0, 0.2, 0.4, 1, 6, and 10 mm shear displacements are presented in Table 2. At the initial stage of shearing and under 0.1 MPa normal stress, the main contact areas includes tiny windows that are just in contact (Fig. 9 mode a). Therefore, it can be stated that the main shear mechanism in these

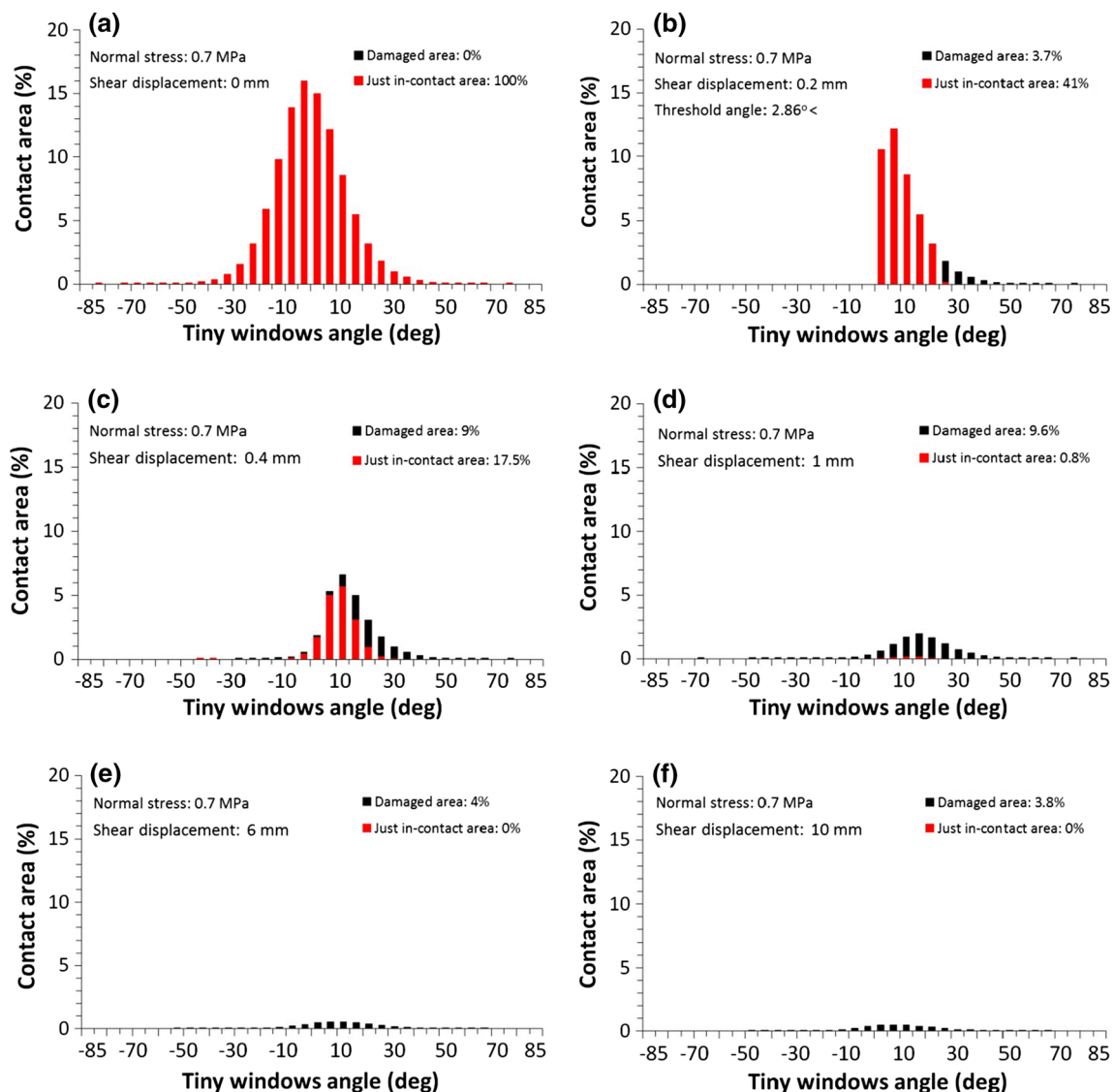


**Fig. 19** Frequency of in-contact tiny windows area versus their angle, under 0.7 MPa normal stress after **a** 0, **b** 0.2, **c** 0.4, **d** 1, **e** 6, and **f** 10 mm shear displacements

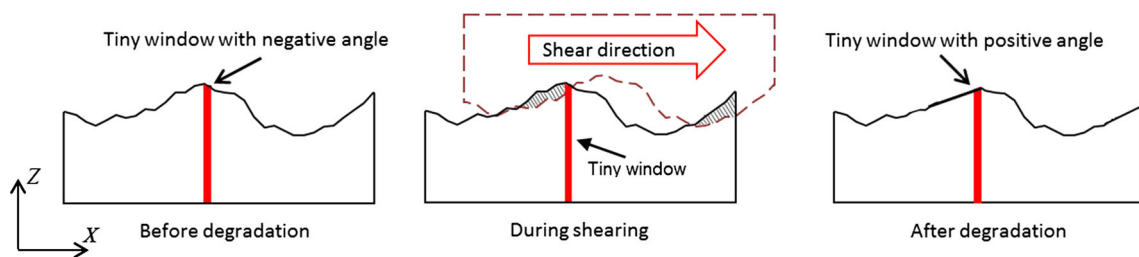


**Fig. 20** The top of some asperities sheared and tiny windows that did not initially face the shear direction (*negative angles*) changed into tiny windows that faced the shear direction (*positive angles*)

**Table 2** Just-in-contact areas and in-contact damaged areas at different shear displacements and under different normal stresses

Normal specimen stress (MPa)	Threshold angles (°) at SD = 0.2 mm		Contact area and damaged areas at different shear displacements (%)												
			0 mm		0.2 mm		0.4 mm		1 mm		6 mm		10 mm		
	ITA	DTA	JCA	DA	JCA	DA	JCA	DA	JCA	DA	JCA	DA	JCA	DA	
A135	0.1	6.3	38.5	100	0	29	0.8	13.3	3.4	0.3	2.8	0	1.1	0	1.0
A137	0.2	5.7	32.4	100	0	30.4	0.9	13	4.5	0.3	3	0	1.3	0	1.1
A139	0.3	4.9	29.2	100	0	31.8	1.8	13.9	5.7	0.3	3	0	1.6	0	1.4
A141	0.4	4.3	27.7	100	0	32.4	2.8	14.3	6.8	0.5	5.4	0	1.9	0	1.5
A142	0.5	3.7	26.6	100	0	36.2	3.2	14.9	7.1	0.5	5.9	0	1.9	0	1.8
A144	0.6	3.1	25.4	100	0	40.1	3.7	16.4	8.0	0.7	8.2	0	3.2	0	2.9
A145	0.7	2.9	25	100	0	41	3.7	17.5	8.7	0.8	9.6	0	4	0	3.8

JCA just-in-contact areas

DA in-contact damaged areas

ITA in-contact threshold angle

DTA damaged threshold angle

situations was the sliding of the tiny windows over each other. Although tiny windows that face the shear direction remained in contact at 0.2 mm shear displacement, the steepest tiny windows started to be deformed and sheared (Fig. 18b). At higher normal stresses where threshold angles decreased, both damaged areas and just-in-contact areas increased.

As shearing starts, the percentage of the just-in-contact areas (JCA) decreases due to (1) non-participation of many of the tiny windows with negative angles in the shear process and (2) dilation. The percentage of the in-contact damaged areas (DA) increases as a result of degradation of the secondary and primary asperities. Then, because of dilation, most damaged areas lose their contact except some specific ones that are still under degradation. That is why the percentage of the in-contact damaged areas decreases after the post-peak period (0.4 or 1 mm shear displacement, depending on applied normal load).

Figure 21 shows how in-contact damaged area and just-in-contact area change by shear displacement.

The effect of normal stress and shear displacement on the total contact area including just-in-contact area and in-

contact damaged area are shown in Fig. 22. This figure shows that the contact area decreases quickly during the pre-peak and post-peak softening stages of shearing. Also, under higher normal stress, larger contact areas were observed due to greater degradation. The tiny windows with a wide range of angles (from negative to positive) remained in contact after the peak, more specifically in the residual section. Therefore, the angle of the tiny windows cannot be considered as a sole criterion for identifying the active tiny windows after the peak shear strength of joints.

#### 4.2 Characterization of In-contact Tiny Windows Based on Their Height

In this section, the height of the tiny windows is considered as another criterion for characterizing the role of the asperities in the shearing process. Tiny windows were sorted into ten height classes from 0 to 10 mm. Figure 23a–f shows the contact area histograms of the tiny windows’ heights under 0.1 MPa normal stress at the initial stage of shearing and after five different shear displacements (0.2, 0.4, 1, 6 and 10 mm).



**Fig. 21** In-contact damaged area and just-in-contact area versus shear displacement under 0.1 and 0.7 MPa normal stresses

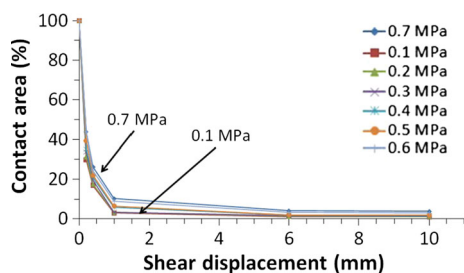
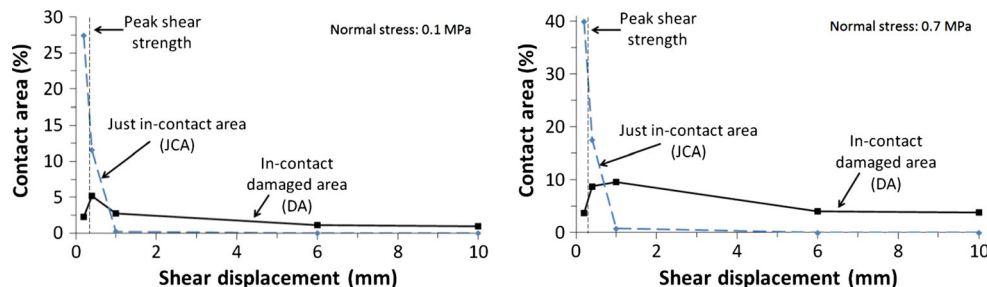


**Fig. 22** Total contact area versus shear displacement under different normal stresses from 0.1 to 0.7 MPa

About 30 % of the tiny windows in each height classes remain in contact after 0.2 mm shear displacement. This value is about 9, 5, 4.6, and 3.5 % after 0.4, 1, 6, and 10 mm shear displacement. Figure 24a–f shows the contact area histograms of the tiny windows' heights under 0.7 MPa normal stress at different shear displacements. These results as well as the results obtained from the shear test under 0.1 MPa normal stress confirm that tiny windows with different heights, not just the highest ones, are in contact in the shear process of the matched specimens. The results also indicated that the percentage of the in-contact tiny windows increased by about 50 % before the peak and 250 % in the residual stage of shearing in each height class when the normal stress increased from 0.1 to 0.7 MPa. Most of the in-contact tiny windows had heights close to the average heights of tiny windows (3.5–4 mm) when shear displacement was less than 1 mm. After 1 mm shear displacement, the heights of in-contact tiny windows were close to the mid-range of the tiny windows' heights (5 mm). The results from characterization of in-contact tiny windows based on their heights illustrated that there was no link between the height and the role of tiny windows in the shearing process.

### 4.3 Characterization of In-contact Tiny Windows Based on Both Their Angles and Heights

The variation of tiny windows at different shear displacements was studied by considering their angles and heights simultaneously. For this purpose, frequency histograms of

tiny windows with the same height and angle were drawn (Fig. 25). As can be seen in Fig. 25, most of the tiny windows exhibited heights between 3 and 6 mm and angles between  $-25^\circ$  and  $25^\circ$ .

To follow the height and angle properties of the in-contact tiny windows at different stages of shearing, the tiny windows that remained in contact after 0, 0.2, 0.4, 1, 6, and 10 mm shear displacements were recorded. Frequency plots (2D view) of tiny windows were drawn instead of frequency histograms (3D view) to provide a better illustration of the in-contact tiny windows. In the frequency plots, colors represent the number of tiny windows. Figures 26 and 27 show the frequency plots of in-contact tiny windows at 0, 0.2, 0.4, 1, 6, and 10 mm shear displacements when normal stress was 0.1 and 0.7 MPa, respectively. At the beginning, the angles of the in-contact tiny windows varied from  $-70^\circ$  to  $70^\circ$  and their heights varied from 0 to 9.31 mm (Figs. 26a, 27a). After 0.2 mm shear displacement, all tiny windows with angles greater than  $6.3^\circ$  when normal stress was 0.1 MPa (Fig. 26b) and greater than  $2.9^\circ$  when normal stress was 0.7 MPa (Fig. 27b) remained in contact. In the post-peak softening stage of shearing when normal stress was 0.1 MPa (Fig. 26d), the main shear mechanism was sliding of asperities over each other, while due to degradation when normal stress was 0.7 MPa (Fig. 27d), tiny windows with negative angles start to participate in the shearing process. As shown in Figs. 26 and 27, in-contact tiny windows had a wide range of angles during the shearing of matched replicas. However, the heights of in-contact tiny windows at the initial stages of shearing varied from 0 to 9.31 mm; mostly tiny windows with a specific range of heights (4.5–5.5 mm) remained in contact in the residual stage of shearing. Although it was expected that the tallest tiny windows would remain in contact of increasing shear displacement, only 11.5 % of in-contact tiny windows had heights between 8 and 9.31 mm. More than 82.3 % of the heights of the in-contact tiny windows in the residual stage of shearing were between 4 and 8 mm. This value was about 6.15 % for those in-contact tiny windows with heights between 2.5 and 4 mm.

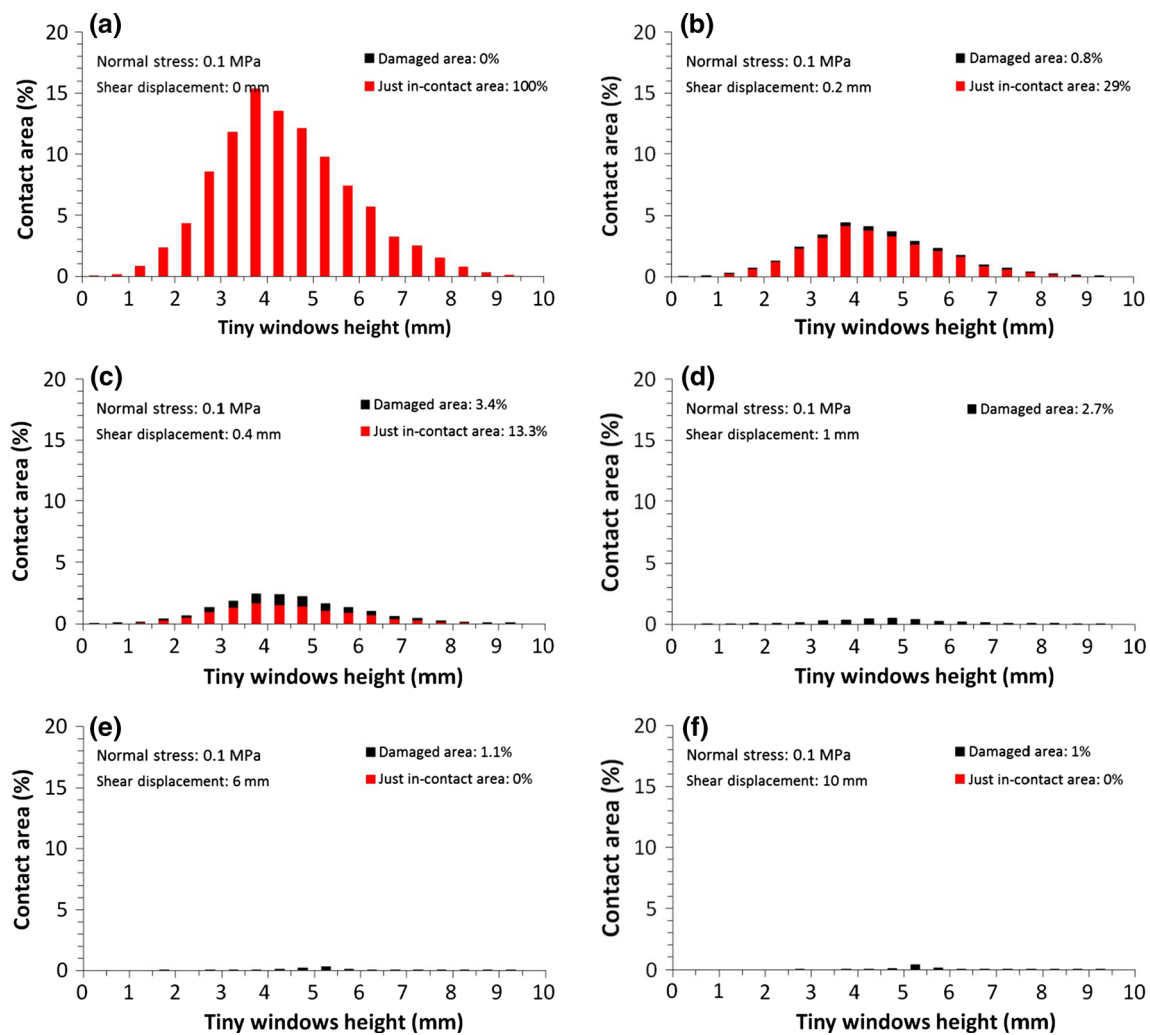


**Fig. 23** Frequency of in-contact tiny windows versus their heights under 0.1 MPa normal stress and after different shear displacements

## 5 Conclusions

In this paper, a new methodology for the geometric characterization of in-contact asperities during the direct shearing test of rock joints was proposed. In the proposed method, the joint surface is divided into a large number of tiny windows. Based on the tiny windows concept, the joint surfaces were reconstructed using a numerical method and contact conditions of tiny windows at different shear displacements were examined. To verify the method, the anticipated damaged areas were compared visually with image analysis results at three different shear displacements. The comparison showed that the location of the estimated damaged areas matched well with those observed by image analysis. This confirmation shows that the proposed method is suitable for detecting damaged areas. Verifying anticipated just-in-contact areas using image analysis method was not possible; however, it was presumed that the proposed method provides a way to identify

just-in-contact tiny windows, though the authors believe that further and more detailed studies are necessary.

The proposed method was applied to the experimental results to track geometric properties of in-contact tiny windows in the shearing process. Results showed that the steepest tiny windows that face the shear direction (positive angles) play a primary role in the shear mechanism. These in-contact tiny windows were divided into two groups: just-in-contact tiny windows and in-contact damaged tiny windows. Before peak, the total contact area includes tiny windows that are just in contact. In this stage, the main shear mechanism is sliding of the tiny windows over each other. The steepest tiny windows start to be deformed and sheared just before the peak. In the post-peak stage of shearing, the participation of just-in-contact tiny windows in the shear process declined sharply. In this stage, the shear mechanism switched from just sliding to sliding and shearing. Due to degradation of asperities, the negative angle of some tiny windows changes to positive and these

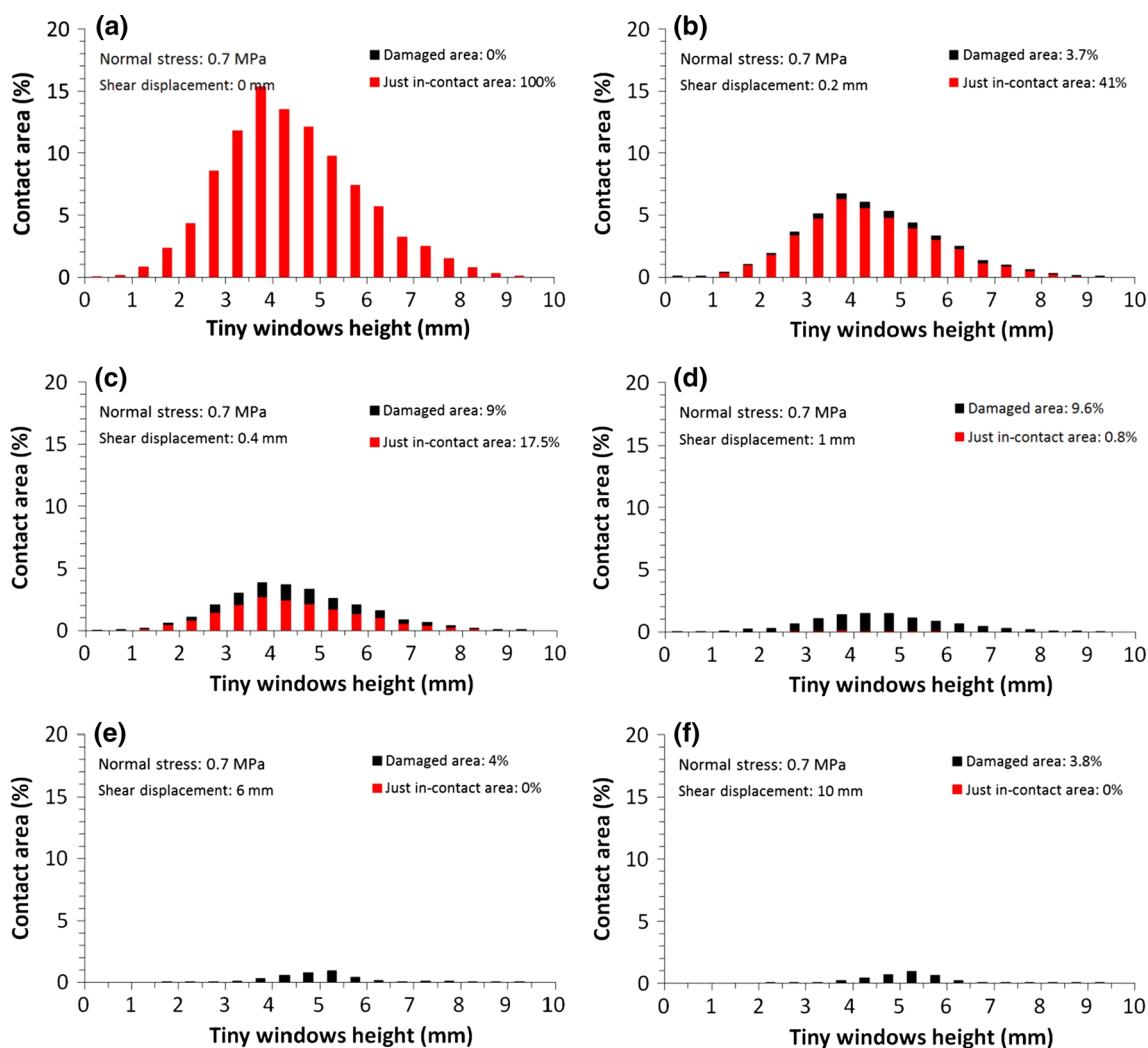


Fig. 24 Frequency of in-contact tiny windows versus their heights under 0.7 MPa normal stress and after different shear displacements

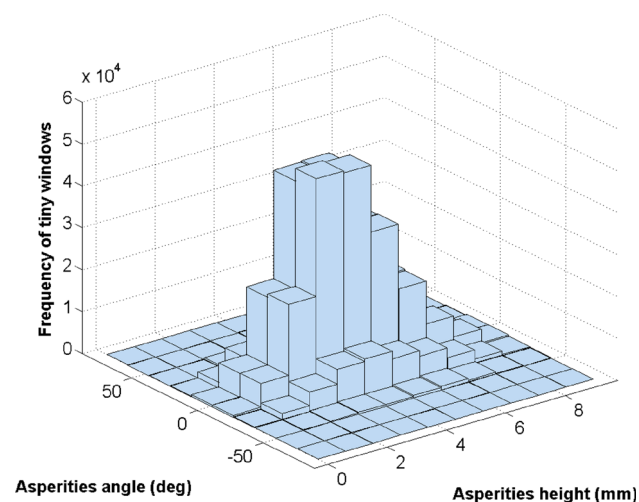
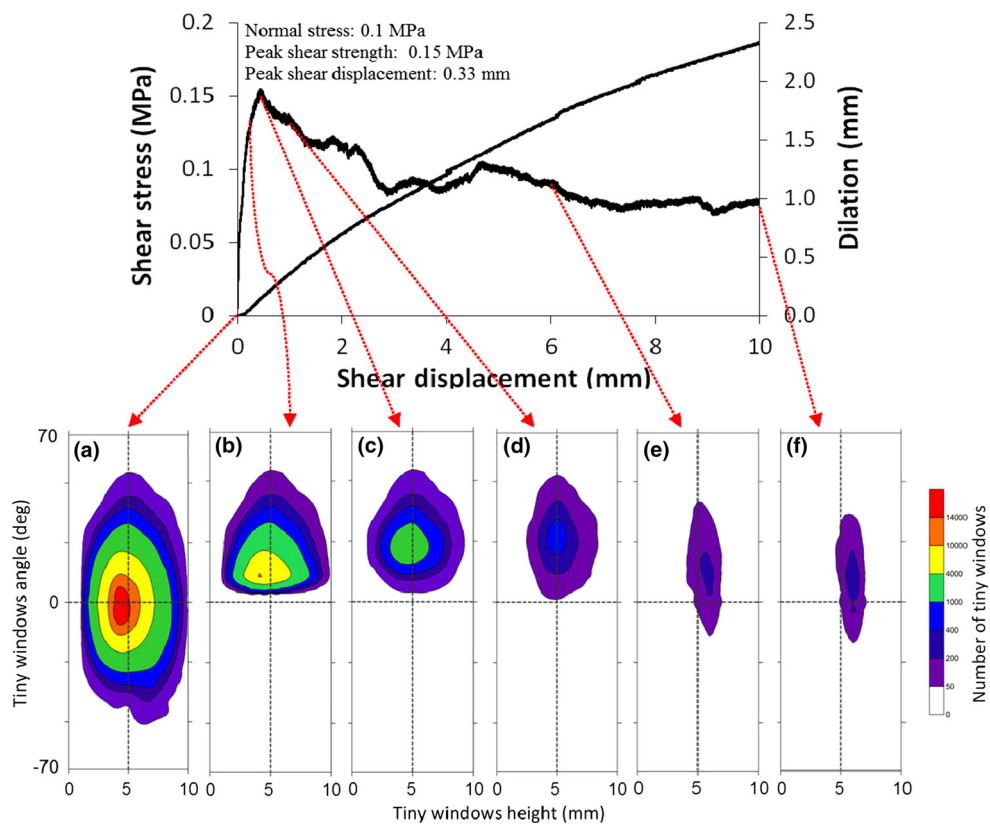


Fig. 25 Frequency histogram of in-contact tiny windows by considering their heights and angles simultaneously

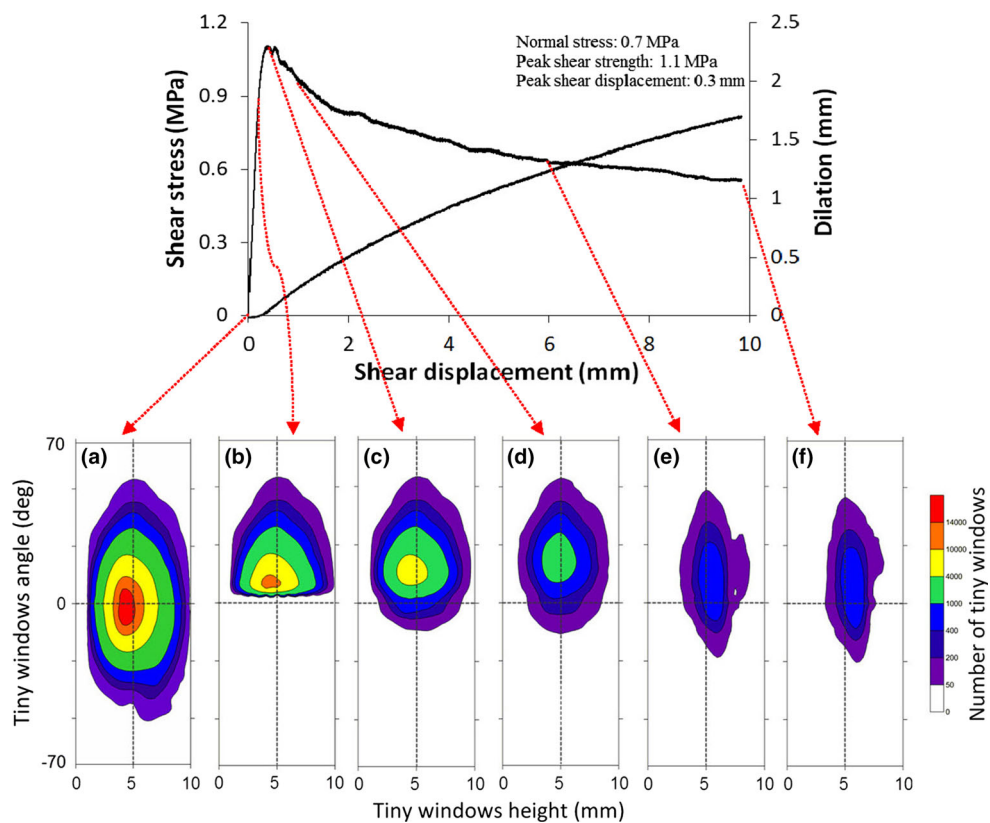
tiny windows then come in contact in the shearing process. Therefore, the tiny windows that remained in contact after the peak have a wide range of angles (from negative to positive). The only tiny windows that remained in contact in the residual stage of shearing were damaged windows. The shear mechanism in this stage is crushing of in-contact tiny windows that are strongly affected by the normal stress and shear displacement. It was observed that tiny windows with different heights participate in the shearing process; however in the residual stage, tiny windows with a specific range of heights remained in contact.

Previous researchers considered contact areas, but did not differentiate between just-in-contact areas and damaged areas. The results of the proposed method indicate that differentiating between these areas will provide greater accuracy in understanding the shear mechanism of the rock joints.

**Fig. 26** Frequency of the in-contact tiny windows after **a** 0, **b** 0.2, **c** 0.4, **d** 1, **e** 6, and **f** 10 mm shear displacements and under 0.1 MPa normal stress by considering their heights and angles



**Fig. 27** Frequency of the in-contact tiny windows after **a** 0, **b** 0.2, **c** 0.4, **d** 1, **e** 6, and **f** 10 mm shear displacements and under 0.7 MPa normal stress by considering their heights and angles



It should be emphasized that these results were obtained from perfectly matched and similar specimens. It is recommended that the proposed method be evaluated by more experiments on natural rock joints which are not perfectly matched.

**Acknowledgments** This research program was made possible by a FONCER-INFRA Grant in partnership with Hydro-Québec. The authors would like to thank Clermont Gravel, Danick Charbonneau, and Ghislaine Luc for their cooperation.

## References

- Barbosa RE (2009) Constitutive model for small rock joint samples in the lab and large rock joint surfaces in the field. In: Diederichs M, Grasselli G (ed) Proceedings of the 3rd CANUS Rock Mechanics Symposium, Toronto
- Barton N (1973) Review of a new shear strength criterion for rock joints. *Eng Geol* 7:287–332
- Barton N, Bandis S (1990) Review of predictive capabilities of JRC–JCS model in engineering practice. In: Proceeding of International Symposium on Rock Joints. Loen Norway, AA Balkema Rotterdam, pp 603–610
- Barton N, Choubey V (1977) The shear strength of rock joints in theory and practice. *Rock Mech Rock Eng* 10(1):1–54
- El Soudani SM (1978) Profilometric analysis of fractures. *Metallography* 11:247–336
- Gentier S, Riss J, Archambault G, Flamand R, Hopkins DL (2000) Influence of fracture geometry on shear behavior. *Int J Rock Mech Min Sci* 37:161–174
- Grasselli G, Egger P (2003) Constitutive law for the shear strength of rock joints based on three-dimensional surface parameters. *Int J Rock Mech Min Sci* 40(1):25–40
- Hakami E, Larsson E (1996) Aperture measurements and flow experiments on a single natural fracture. *Int J Rock Mech Min Sci* 33(4):395–404
- Huang TH, Chang CS, Chao CY (2002) Experimental and mathematical modeling for fracture of rock joint with regular asperities. *Eng Fract Mech* 69:1977–1996
- Hutson RW, Dowding CH (1990) Joint asperity degradation during cyclic shear. *Int J Rock Mech Min Sci Geomech Abstr* 27(2):109–119
- Karami A, Stead D (2008) Asperity degradation and damage in direct shear test: a hybrid FEM/DEM approach. *Rock Mech Rock Engng.* 41(2):229–266
- Kulatilake PHSW, Shou G, Huang TH, Morgan RM (1995) New peak shear strength criterion for anisotropic rock joints. *Int J Rock Mech Min Sci Geomech Abstr* 32(7):673–697
- Ladanyi B, Archambault G (1970) Simulation of shear behaviour of a jointed rock mass. In: Proceeding of 11th US Syrup Rock Mech, pp 105–125
- Lopez P, Riss J, Archambault G (2003) An experimental design linking morphology to the mechanical behavior of shear fracture surfaces. *Int J Rock Mech Min Sci* 40(6):947–954
- Misra A (2002) Effect of asperity damage on shear behaviour of single fracture. *Eng Fract Mech* 69:1997–2014
- Moradian ZA, Ballivy G, Rivard P, Gravel C, Rousseau B (2010) Evaluating damage during shear tests of rock joints using acoustic emission. *Int J Rock Mech Min Sci* 47(4):590–598
- Moradian ZA, Ballivy G, Rivard P (2012) Correlation between acoustic emission source locations and damage zones of rock joints under direct shear test. *Can Geotech J* 49(6):710–718
- Mouchaorab K, Benmokrane B (1994) A new combined servo-controlled testing machine—direct shear apparatus for the study of concrete joint behaviour under different boundary and loading conditions. *ASTM J Geotech Test* 17(2):233–242
- Myers NO (1962) Characterization of surface roughness. *Wear* 5:182–189
- Nemoto K, Watanabe N, Hirano N, Tsuchiya N (2009) Direct measurement of contact area and stress dependence of anisotropic flow through rock fracture with heterogeneous aperture distribution. *Earth Planet Sci Lett* 281:81–87
- Park JW, Song JJ (2013) Numerical method for the determination of contact areas of a rock joint under normal and shear loads. *Int J Rock Mech Min Sci* 58:8–22
- Patton FD (1966) Multiple modes of shear failure in rock. In: Proceeding 1st Cong Int Soc Rock Mech 1:509–513
- Pyrak-Nolte LJ, Myer LR, Cook NGW, Witherspoon PA (1987) Hydraulic and mechanical properties of natural fractures in low permeability rock. In: Proceedings of the 6th congress international society for rock mechanics. Montreal 1:225–231
- Re F, Scavia C (1999) Determination of contact areas in rock joints by X-ray computer tomography. *Int J Rock Mech Min Sci* 36(7):883–890
- Rengers N (1970) Influence of surface roughness on the friction properties of rock planes. *Congress of the International Society of Rock Mechanics*:229–234
- Riss J, Gentier S, Sirieix C, Archambault G, Flamand R (1997) Sheared rock joints: dependence of damage zones on morphological anisotropy. *Int J Rock Mech Min Sci* 34(4):258
- Rousseau B, Rivard P, Marache A, Ballivy G, Riss J (2012) Limitations of laser profilometer limitations in measuring surface topography for polycrystalline rocks. *Int J Rock Mech Min Sci* 52:56–60
- Seidel JP, Haberfield CM (1995) The application of energy principles to the determination of the sliding resistance of rock joints. *Int J Rock Mech Rock Eng* 28(4):211–226
- Seidel JP, Haberfield CM (2002) A theoretical model for rock joints subjected to constant normal stiffness direct shear. *J Rock Mech Min Sci* 39(5):539–554
- Tatone BSA, Grasselli G (2010) A new 2D discontinuity roughness parameter and its correlation with JRC. *Int J Rock Mech Min Sci* 47:1391–1400
- Tse R, Cruden DM (1979) Estimating joint roughness coefficients. *Int J Rock Mech Min Sci Geomech Abstr* 16:303–307
- Yang ZY, Di CC, Yen KC (2001) The effect of asperity order on the roughness of rock joints. *Int J Rock Mech Min Sci* 38:745–752
- Zhao J (1997) Joint surface matching and shear strength—part A: joint matching coefficient (JMC). *Int J Rock Mech Min Sci* 34(2):173–178